

Decay $B_s \rightarrow \phi \ell^+ \ell^-$ in covariant quark model

S. Dubnička,¹ A.Z. Dubničková,² A. Issadykov,^{3,4}

M.A. Ivanov,^{3,*} A. Liptaj,^{1,†} and S.K. Sakhiyev^{4,5}

¹*Institute of Physics, Slovak Academy of Sciences, Bratislava, Slovakia*

²*Comenius University, Bratislava, Slovakia*

³*Joint Institute for Nuclear Research, Dubna, Russia*

⁴*Faculty of physics and technical sciences,*

L.N.Gumilyov Eurasian National University,

010008 Astana, Republic of Kazakhstan

⁵*Institute of Nuclear Physics, 050032 Almaty, Republic of Kazakhstan*

Abstract

Our article is devoted to the study of the rare $B_s \rightarrow \phi \ell^+ \ell^-$ decay where $\ell = \mu, \tau$. We compute the relevant form factors in the framework of the covariant quark model with infrared confinement in the full kinematical momentum transfer region. The calculated form factors are used to evaluate branching fractions and polarization observables in the cascade decay $B \rightarrow \phi(\rightarrow K^+ K^-) \ell^+ \ell^-$. We compare the obtained results with available experimental data and the results from other theoretical approaches.

PACS numbers:

Keywords: relativistic quark model, confinement, B-meson, decay widths, polarization observables

*Electronic address: ivanovm@theor.jinr.ru

†Electronic address: andrej.liptaj@savba.sk

I. INTRODUCTION

The transition $b \rightarrow s\ell^+\ell^-$ mediated by Flavor-Changing Neutral Current (FCNC) is one of the key points in the Standard Model (SM) which allows one to look for the possible manifestation of New Physics (NP). The physical processes induced by this transition are currently studied in great details at the LHC. The most popular and well-analyzed among them are the rare B-meson decays $B \rightarrow K^*(\rightarrow K\pi)\mu^+\mu^-$ and $B_s \rightarrow \phi(\rightarrow K^+K^-)\mu^+\mu^-$. The decay $\Lambda_b \rightarrow \Lambda(\rightarrow p\pi)\ell^+\ell^-$ can be considered to be a welcome complement to the above decay channels.

The LHCb Collaboration [1] reported a measurement of form-factor independent angular observables in the decay $B \rightarrow K^*\mu^+\mu^-$. One observable was found to be in disagreement with the SM on the level of 3.7σ .

The improved measurements of the isospin asymmetries and branching fractions for $B \rightarrow K\mu^+\mu^-$ and $B \rightarrow K^*\mu^+\mu^-$ decays were reported in [2]. The isospin asymmetries were consistent with the SM, whereas some branching fractions were found to be slightly lower than the theoretical predictions.

An angular analysis and a measurement of the differential branching fraction of the decay $B_s^0 \rightarrow \phi\mu^+\mu^-$ were presented in [3]. The results of the angular analysis are consistent with the SM. However, the differential branching fraction in one bin was found to be more than 3σ below the SM predictions.

The observed discrepancies (sometimes called “ $b \rightarrow s\ell\ell$ anomalies”) have generated a plenty of theoretical studies [4]-[15] involving the various scenarios of NP and analysis of the uncertainties from hadronic contributions. The form factors obtained from unquenched lattice QCD [16] were used in [17, 18] to calculate the differential branching fractions of the decays $B \rightarrow K^*\mu^+\mu^-$ and $B_s \rightarrow \phi\mu^+\mu^-$.

In this paper we calculate all form factors which appear in the $B_s \rightarrow \phi$ transition by using the covariant quark model. The expressions for the Wilson coefficients C_7 and C_9 are taken on the two-loop level of accuracy by using the results obtained in Refs. [19, 20]. Then we evaluate the branching fraction, the forward-backward asymmetry and the so-called optimized observables in the cascade decay $B_s \rightarrow \phi(\rightarrow K^+K^-)\mu^+\mu^-$. We compare our results with the recent experimental data reported in Ref. [3] for various q^2 -bins.

II. MODEL

The covariant confined quark model [21–24] is an effective quantum field approach to hadronic interactions based on an interaction Lagrangian of hadrons interacting with their constituent quarks. The value of the coupling constant follows from the compositeness condition $Z_H = 0$, where Z_H is the wave function renormalization constant of the hadron. Matrix elements of the physical processes are generated by a set of quark loop diagrams according to the $1/N_c$ expansion. The ultraviolet divergences of the quark loops are regularized by including vertex functions for the hadron-quark vertices. These functions also describe finite size effects related to the non-pointlike hadrons. The quark confinement [24] is built-in through an infrared cutoff on the upper limit of the scale integration to avoid the appearance of singularities in matrix elements. The infrared cutoff parameter λ is universal for all processes. The covariant confined quark model has limited number of parameters: the light and heavy constituent quark masses, the size parameters which describe the size of the distribution of the constituent quarks inside the hadron and the infrared cutoff parameter λ . They are determined by a fit to available experimental data.

Let us start with the effective Lagrangian describing the transition of a meson $M(q_1\bar{q}_2)$ to its constituent quarks q_1 and \bar{q}_2

$$\begin{aligned}\mathcal{L}_{\text{int}}(x) &= g_M M(x) \cdot J_M(x) + \text{h.c.}, \\ J_M(x) &= \int dx_1 \int dx_2 F_M(x, x_1, x_2) \bar{q}_2(x_2) \Gamma_M q_1(x_1)\end{aligned}\quad (1)$$

with Γ_M a Dirac matrix which projects onto the spin quantum number of the meson field $M(x)$. The vertex function F_M characterizes the finite size of the meson. Translational invariance requires the function F_M to fulfill the identity $F_M(x + a, x_1 + a, x_2 + a) = F_M(x, x_1, x_2)$ for any four-vector a . A specific form for the vertex function is adopted

$$F_M(x, x_1, x_2) = \delta(x - w_1 x_1 - w_2 x_2) \Phi_M((x_1 - x_2)^2), \quad (2)$$

where Φ_M is the correlation function of the two constituent quarks with masses m_{q_1} , m_{q_2} and the mass ratios $w_i = m_{q_i}/(m_{q_1} + m_{q_2})$.

A simple Gaussian form of the vertex function $\bar{\Phi}_M(-k^2)$ is selected

$$\bar{\Phi}_M(-k^2) = \exp(k^2/\Lambda_M^2) \quad (3)$$

with the parameter Λ_M linked to the size of the meson. The minus sign in the argument is chosen to indicate that we are working in the Minkowski space. Since k^2 turns into $-k_E^2$ in the Euclidean space, the form (3) has the appropriate fall-off behavior in the Euclidean region. Any choice for Φ_M is appropriate as long as it falls off sufficiently fast in the ultraviolet region of the Euclidean space to render the corresponding Feynman diagrams ultraviolet finite. We choose a Gaussian form for calculational convenience.

The fermion propagators for the quarks are given by

$$S_i(k) = \frac{1}{m_{q_i} - \not{k}} \quad (4)$$

with an effective constituent quark mass m_{q_i} .

The so-called *compositeness condition* [22, 25–27] is used to determine the value of the coupling constants g_M . It means that the renormalization constant Z_M of the elementary meson field $M(x)$ is set to zero, i.e.,

$$Z_M = 1 - \frac{3g_M^2}{4\pi^2} \bar{\Pi}'_M(m_M^2) = 0, \quad (5)$$

where $\bar{\Pi}'_M$ is the derivative of the meson mass operator. Its physical meaning in Eq. (5) becomes clear when interpreted as the matrix element between the physical and the corresponding bare state: $Z_M = 0$ implies that the physical state does not contain the bare state and is appropriately described as a bound state. The interaction makes the physical particle dressed, i.e. its mass and wave function have to be renormalized. The condition $Z_M = 0$ also effectively excludes the constituent degrees of freedom from the space of physical states. It thereby guarantees the absence of double counting for the physical observable under consideration, the constituents exist only in virtual states. The tree-level diagram together with the diagrams containing self-energy insertions into the external legs (i.e. the tree-level diagram times $Z_M - 1$) give a common factor Z_M which is equal to zero.

The mass functions for the pseudoscalar meson (spin $S = 0$) and vector meson (spin $S = 1$) are defined as

$$\Pi_P(x - y) = +i \langle T \{ J_P(x) J_P(y) \} \rangle_0, \quad (6)$$

$$\Pi_V^{\mu\nu}(x - y) = -i \langle T \{ J_V^\mu(x) J_V^\nu(y) \} \rangle_0. \quad (7)$$

By using the Fourier transforms of the vertex functions in Eq. (3) and quark propagators in

Eq.(4) one can easily find the Fourier transforms of the mass functions

$$\tilde{\Pi}_P(p^2) = N_c \int \frac{d^4k}{(2\pi)^{4i}} \tilde{\Phi}_P^2(-k^2) \text{tr} \left(\gamma^5 S_1(k + w_1 p) \gamma^5 S_2(k - w_2 p) \right), \quad (8)$$

$$\begin{aligned} \tilde{\Pi}_V^{\mu\nu}(p) &= N_c \int \frac{d^4k}{(2\pi)^{4i}} \tilde{\Phi}_V^2(-k^2) \text{tr} \left(\gamma^\mu S_1(k + w_1 p) \gamma^\nu S_2(k - w_2 p) \right) \\ &= g^{\mu\nu} \tilde{\Pi}_V(p^2) + p^\mu p^\nu \tilde{\Pi}_V^{\parallel}(p^2) \end{aligned} \quad (9)$$

where $N_c = 3$ is the number of colors. Due to the transversality of the vector field the second term in Eq. (9) is irrelevant in our consideration. The first term in Eq. (9) may be picked out as

$$\tilde{\Pi}_V(p^2) = \frac{1}{3} \left(g_{\mu\nu} - \frac{p_\mu p_\nu}{p^2} \right) \tilde{\Pi}_V^{\mu\nu}(p). \quad (10)$$

The loop integrations in Eqs. (8) and (9) are done with the help of the Fock-Schwinger representation of the quark propagator

$$\begin{aligned} S_q(k+p) &= \frac{1}{m_q - \not{k} - \not{p}} = \frac{m_q + \not{k} + \not{p}}{m_q^2 - (k+p)^2} \\ &= (m_q + \not{k} + \not{p}) \int_0^\infty d\alpha e^{-\alpha[m_q^2 - (k+p)^2]}, \end{aligned} \quad (11)$$

where k is the loop momentum and p is the external momentum. As described later on, the use of the Fock-Schwinger representation allows one to do tensor loop integrals in a very efficient way since one can convert loop momenta into derivatives of the exponential function.

All loop integrations are performed in Euclidean space. The transition from Minkowski space to Euclidean space is performed by using the Wick rotation

$$k_0 = e^{i\frac{\pi}{2}} k_4 = ik_4 \quad (12)$$

so that $k^2 = k_0^2 - \vec{k}^2 = -k_4^2 - \vec{k}^2 = -k_E^2 \leq 0$. Simultaneously one has to rotate all external momenta, i.e. $p_0 \rightarrow ip_4$ so that $p^2 = -p_E^2 \leq 0$. Then the quadratic form in Eq. (11) becomes positive-definite

$$m_q^2 - (k+p)^2 = m_q^2 + (k_E + p_E)^2 > 0,$$

and the integral over α is absolutely convergent. We will keep the Minkowski notation to avoid excessive relabeling. We simply imply that $k^2 \leq 0$ and $p^2 \leq 0$.

Collecting the representations for the vertex functions and quark propagators given by Eqs. (3) and (11), respectively, one can perform the Gaussian integration in the expressions for the matrix elements in Eqs. (8) and (9). The exponent has the form $ak^2 + 2kr + z_0$, where $r = bp$. Using the following properties

$$\begin{aligned} k^\mu \exp(ak^2 + 2kr + z_0) &= \frac{1}{2} \frac{\partial}{\partial r_\mu} \exp(ak^2 + 2kr + z_0) \\ k^\mu k^\nu \exp(ak^2 + 2kr + z_0) &= \frac{1}{2} \frac{\partial}{\partial r_\mu} \frac{1}{2} \frac{\partial}{\partial r_\nu} \exp(ak^2 + 2kr + z_0) \end{aligned} \quad (13)$$

etc.

one can replace k by $\not{\partial}_r = \gamma^\mu \frac{\partial}{\partial r_\mu}$ which allows one to exchange the tensor integrations for a differentiation of the Gaussian exponent $e^{-r^2/a}$ which appears after integration over loop momentum. The r -dependent Gaussian exponent $e^{-r^2/a}$ can be moved to the left through the differential operator $\not{\partial}_r$ by using the following properties

$$\begin{aligned} \frac{\partial}{\partial r_\mu} e^{-r^2/a} &= e^{-r^2/a} \left[-\frac{2r^\mu}{a} + \frac{\partial}{\partial r_\mu} \right], \\ \frac{\partial}{\partial r_\mu} \frac{\partial}{\partial r_\nu} e^{-r^2/a} &= e^{-r^2/a} \left[-\frac{2r^\mu}{a} + \frac{\partial}{\partial r_\mu} \right] \cdot \left[-\frac{2r^\nu}{a} + \frac{\partial}{\partial r_\nu} \right], \end{aligned} \quad (14)$$

etc.

Finally, one has to move the derivatives to the right by using the commutation relation

$$\left[\frac{\partial}{\partial r_\mu}, r^\nu \right] = g^{\mu\nu}. \quad (15)$$

The last step has been done by using a FORM code which works for any numbers of loops and propagators. In the remaining integrals over the Fock-Schwinger parameters $0 \leq \alpha_i < \infty$ we introduce an additional integration which converts the set of Fock-Schwinger parameters into a simplex. We use the transformation:

$$\prod_{i=1}^n \int_0^\infty d\alpha_i f(\alpha_1, \dots, \alpha_n) = \int_0^\infty dt t^{n-1} \prod_{i=1}^n \int d\alpha_i \delta \left(1 - \sum_{i=1}^n \alpha_i \right) f(t\alpha_1, \dots, t\alpha_n) \quad (16)$$

Finally, one finds

$$\tilde{\Pi}_M(p^2) = \frac{3}{4\pi^2} \int_0^\infty dt t \int_0^1 d\alpha e^{-t z_0 + z_M} \left\{ \frac{n_M}{a_M} + m_{q_1} m_{q_2} + \left(w_1 - \frac{b}{a_M} \right) \left(w_2 + \frac{b}{a_M} \right) p^2 \right\} \quad (17)$$

$$z_0 = \alpha m_{q_1}^2 + (1 - \alpha) m_{q_2}^2 - \alpha(1 - \alpha) p^2, \quad z_M = \frac{2s_M t}{2s_M + t} (\alpha - w_2)^2 p^2,$$

$$a_M = 2s_M + t, \quad b = (\alpha - w_2) t.$$

Here $n_M = 2$ for a pseudoscalar and $n_M = 1$ for vector particle. The parameter s_M is related to the size parameter Λ_M as $s_M = 1/\Lambda_M^2$.

The integral over “ t ” is well-defined and convergent below the threshold $p^2 < (m_{q_1} + m_{q_2})^2$. The convergence of the integral above threshold $p^2 \geq (m_{q_1} + m_{q_2})^2$ is guaranteed by the addition of a small imaginary part to the quark mass, i.e. $m_q \rightarrow m_q - i\epsilon$, $\epsilon > 0$ in the quark propagator. It allows one to rotate the integration variable “ t ” to the imaginary axis $t \rightarrow it$. As a result the integral becomes convergent but obtains an imaginary part corresponding to quark pair production.

However, by cutting the scale integration at the upper limit, which corresponds to the introduction of an infrared cutoff

$$\int_0^\infty dt(\dots) \rightarrow \int_0^{1/\lambda^2} dt(\dots) \quad (18)$$

one can remove all possible thresholds present in the initial quark diagram [24]. Thus the infrared cutoff parameter λ effectively guarantees the confinement of quarks within hadrons. This method is quite general and can be used for diagrams with an arbitrary number of loops and propagators.

III. FORM FACTORS OF THE $B_s \rightarrow \phi$ TRANSITION

The Feynman diagram describing the $B_s \rightarrow \phi$ transition in the framework of our covariant quark model is depicted in Fig. 1. The matrix element is expressed through dimensionless form factors [28, 29]:

$$\begin{aligned} & \langle \phi(p_2, \epsilon_2) | \bar{s} O^\mu b | B_s(p_1) \rangle = \\ & = N_c g_{B_s} g_\phi \int \frac{d^4 k}{(2\pi)^4 i} \tilde{\Phi}_{B_s} \left(- (k + w_{13} p_1)^2 \right) \tilde{\Phi}_\phi \left(- (k + w_{23} p_2)^2 \right) \\ & \times \text{tr} \left[O^\mu S_b(k + p_1) \gamma^5 S_s(k) \not{\epsilon}_2^\dagger S_s(k + p_2) \right] \\ & = \frac{\epsilon_\nu^\dagger}{m_1 + m_2} \left(- g^{\mu\nu} P \cdot q A_0(q^2) + P^\mu P^\nu A_+(q^2) + q^\mu P^\nu A_-(q^2) \right. \\ & \left. + i \varepsilon^{\mu\nu\alpha\beta} P_\alpha q_\beta V(q^2) \right), \end{aligned} \quad (19)$$

$$\begin{aligned}
& \langle \phi(p_2, \epsilon_2) | \bar{s} (\sigma^{\mu\nu} q_\nu (1 + \gamma^5)) b | B_s(p_1) \rangle = \\
& = N_c g_{B_s} g_\phi \int \frac{d^4 k}{(2\pi)^4 i} \tilde{\Phi}_{B_s} \left(- (k + w_{13} p_1)^2 \right) \tilde{\Phi}_\phi \left(- (k + w_{23} p_2)^2 \right) \\
& \times \text{tr} \left[(\sigma^{\mu\nu} q_\nu (1 + \gamma^5)) S_b(k + p_1) \gamma^5 S_s(k) \not{\epsilon}_2^\dagger S_s(k + p_2) \right] \\
& = \epsilon_\nu^\dagger \left(- (g^{\mu\nu} - q^\mu q^\nu / q^2) P \cdot q a_0(q^2) + (P^\mu P^\nu - q^\mu P^\nu P \cdot q / q^2) a_+(q^2) \right. \\
& \quad \left. + i \varepsilon^{\mu\nu\alpha\beta} P_\alpha q_\beta g(q^2) \right). \tag{20}
\end{aligned}$$

Here, $P = p_1 + p_2$, $q = p_1 - p_2$, $\epsilon_2^\dagger \cdot p_2 = 0$, $p_1^2 = m_1^2 \equiv m_{B_s}^2$, $p_2^2 = m_2^2 \equiv m_\phi^2$ and the weak matrix $O^\mu = \gamma^\mu(1 - \gamma^5)$. Since there are three quarks involved in these processes, we introduce the notation with two subscripts $w_{ij} = m_{q_j}/(m_{q_i} + m_{q_j})$ ($i, j = 1, 2, 3$) so that $w_{ij} + w_{ji} = 1$. The form factors defined in Eq. (20) satisfy the physical requirement $a_0(0) = a_+(0)$, which ensures that no kinematic singularity appears in the matrix element at $q^2 = 0 \text{ GeV}^2$.

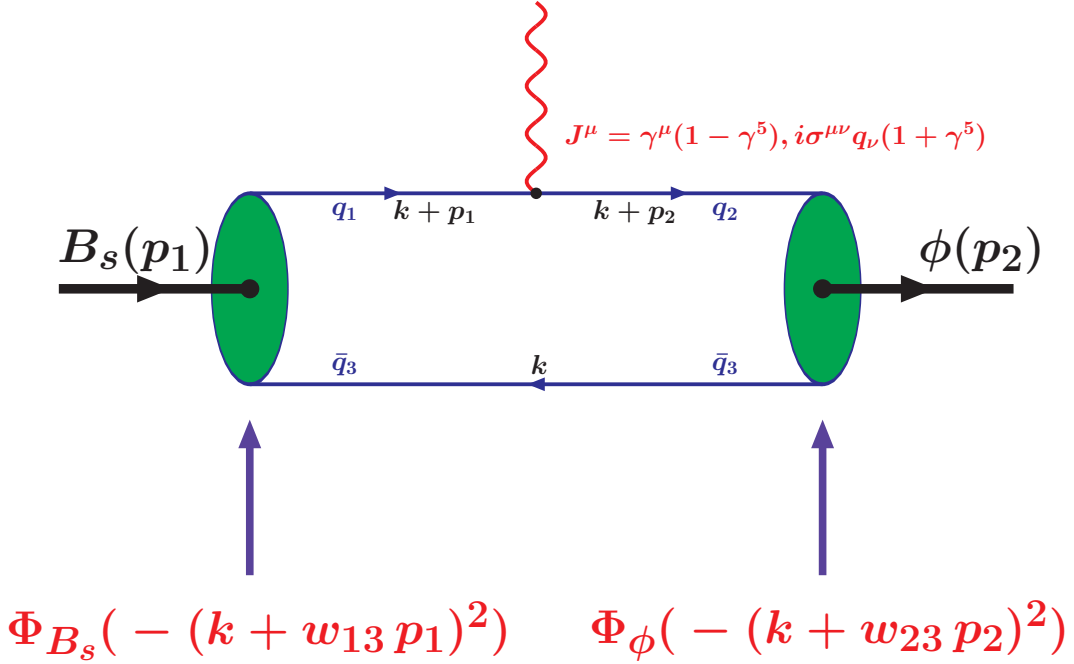


FIG. 1: Diagrammatic representation of the matrix elements describing $B_s \rightarrow \phi$ transitions. Identification of quarks: $q_1 = b$, $q_2 = q_3 = s$, $w_{13} = m_s/(m_b + m_s)$ and $w_{23} = 1/2$.

Herein we use the updated values of the model parameters [28] which are shown in

Eq. (21).

$m_{u/d}$	m_s	m_c	m_b	λ	Λ_{B_s}	Λ_ϕ	
0.241	0.428	1.67	5.05	0.181	2.05	0.88	GeV

(21)

Performing the loop integration in Eqs. (19) and (20) in a manner described in the previous section, one can obtain the form factors in the form of three-fold integrals which are calculated numerically by using the FORTRAN code with NAG library. The form factors are calculated in the full kinematical region of momentum transfer squared. The curves are depicted in Fig. 2.

The results of our numerical calculations are with high accuracy approximated by the parametrization

$$F(q^2) = \frac{F(0)}{1 - as + bs^2}, \quad s = \frac{q^2}{m_1^2}, \quad (22)$$

the relative error is less than 1%. The values of $F(0)$, a , and b are listed in Table I.

TABLE I: Parameters for the approximated form factors in Eq. (22).

	A_0	A_+	A_-	V	a_0	a_+	g
$F(0)$	0.40	0.27	-0.29	0.31	0.27	0.27	0.27
a	0.62	1.41	1.48	1.51	0.66	1.41	1.52
b	-0.30	0.38	0.45	0.47	-0.26	0.39	0.49

For reference it is useful to relate the above form factors to those used, e.g., in Ref. [30] (we denote them by the superscript c). The relations read

$$\begin{aligned}
A_0 &= \frac{m_1 + m_2}{m_1 - m_2} A_1^c, & A_+ &= A_2^c, \\
A_- &= \frac{2m_2(m_1 + m_2)}{q^2} (A_3^c - A_0^c), & V &= V^c, \\
a_0 &= T_2^c, & g &= T_1^c, & a_+ &= T_2^c + \frac{q^2}{m_1^2 - m_2^2} T_3^c.
\end{aligned} \quad (23)$$

We note in addition that the form factors (23) satisfy the constraints

$$\begin{aligned}
A_0^c(0) &= A_3^c(0) \\
2m_2 A_3^c(q^2) &= (m_1 + m_2) A_1^c(q^2) - (m_1 - m_2) A_2^c(q^2).
\end{aligned} \quad (24)$$

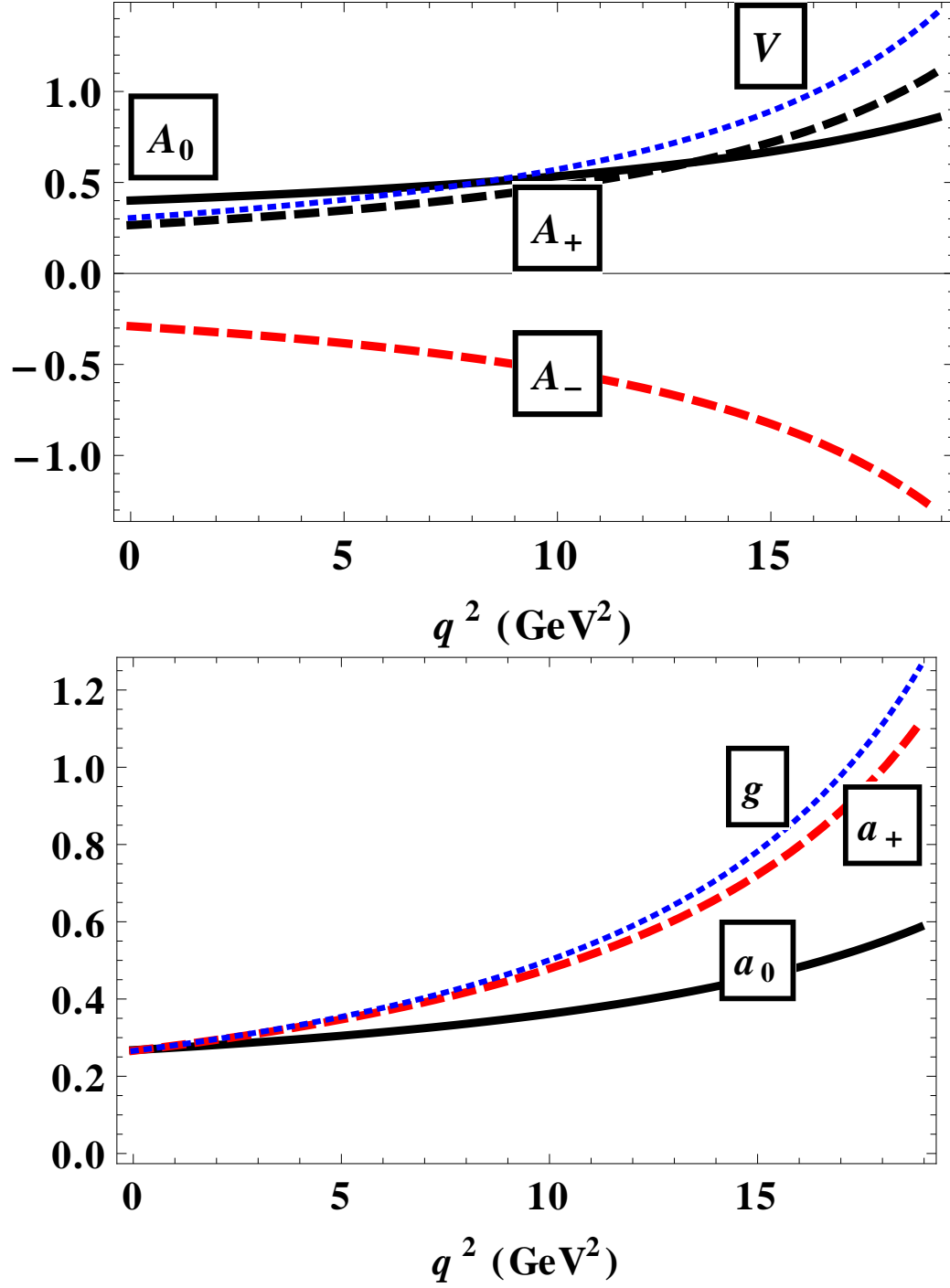


FIG. 2: The q^2 -dependence of the vector and axial form factors (upper plot) and tensor form factors (lower plot).

TABLE II: The form factors at maximum recoil $q^2 = 0$.

	$V^c(0)$	$A_0^c(0)$	$A_1^c(0)$	$A_2^c(0)$	$T_1^c(0)$	$T_3^c(0)$
This work	0.31 ± 0.03	0.28 ± 0.03	0.27 ± 0.03	0.27 ± 0.03	0.27 ± 0.03	0.18 ± 0.02
Ref. [29]	0.32		0.29	0.28	0.28	
Ref. [31]	0.434 ± 0.035	0.474 ± 0.037	0.311 ± 0.029	0.234 ± 0.028	0.349 ± 0.033	0.175 ± 0.018
Ref. [32]	0.406 ± 0.020	0.322 ± 0.016	0.320 ± 0.016	0.318 ± 0.016	0.275 ± 0.014	0.133 ± 0.006
Ref. [33]	0.43	0.38	0.30	0.26	0.35	0.25
Ref. [34]	0.25 ± 0.05	0.30 ± 0.05	0.19 ± 0.04			
Ref. [35]	0.44	0.42	0.34	0.31	0.38	0.26
Ref. [36]	0.26 ± 0.07	0.31 ± 0.07	$0.18_{-0.05}^{+0.06}$	0.12 ± 0.03	$0.23_{-0.05}^{+0.06}$	0.19 ± 0.05
Ref. [37]	0.329	0.279	0.232	0.210	0.276	0.170
Ref. [38]	0.339 ± 0.017		0.271 ± 0.014	0.212 ± 0.011	0.299 ± 0.016	0.191 ± 0.010

Since $a_0(0) = a_+(0) = g(0)$ we display in Table II the form factors $A_0^c(0) = (m_1 - m_2)[A_0(0) - A_+(0)]/(2m_2)$, $A_1^c(0) = A_0(0)(m_1 - m_2)/(m_1 + m_2)$, $A_2^c(0) = A_+(0)$, $T_1^c(0) = g(0)$ and $T_3^c(0) = \lim_{q^2 \rightarrow 0} (m_1^2 - m_2^2)(a_+ - a_0)/q^2$ obtained in our model and compare them with those from other approaches.

IV. EFFECTIVE HAMILTONIAN

The rare decay $b \rightarrow sl^+\ell^-$ is described in terms of the effective Hamiltonian [39]:

$$\mathcal{H}_{\text{eff}} = -\frac{4G_F}{\sqrt{2}}\lambda_t \sum_{i=1}^{10} C_i(\mu)\mathcal{O}_i(\mu), \quad (25)$$

where $C_i(\mu)$ and $\mathcal{O}_i(\mu)$ are the Wilson coefficients and local operators, respectively. $\lambda_t = |V_{tb}V_{ts}^*|$ is the product of Cabibbo-Kobayashi-Maskawa (CKM) matrix elements. Note that we drop small corrections proportional to $\lambda_u = |V_{ub}V_{us}^*|$. The standard set [39] of local operators obtained within the SM for $b \rightarrow sl^+\ell^-$ transition is written as

$$\begin{aligned}
\mathcal{O}_1 &= (\bar{s}_{a_1} \gamma^\mu P_L c_{a_2})(\bar{c}_{a_2} \gamma_\mu P_L b_{a_1}), & \mathcal{O}_2 &= (\bar{s} \gamma^\mu P_L c)(\bar{c} \gamma_\mu P_L b), \\
\mathcal{O}_3 &= (\bar{s} \gamma^\mu P_L b) \sum_q (\bar{q} \gamma_\mu P_L q), & \mathcal{O}_4 &= (\bar{s}_{a_1} \gamma^\mu P_L b_{a_2}) \sum_q (\bar{q}_{a_2} \gamma_\mu P_L q_{a_1}), \\
\mathcal{O}_5 &= (\bar{s} \gamma^\mu P_L b) \sum_q (\bar{q} \gamma_\mu P_R q), & \mathcal{O}_6 &= (\bar{s}_{a_1} \gamma^\mu P_L b_{a_2}) \sum_q (\bar{q}_{a_2} \gamma_\mu P_R q_{a_1}), \\
\mathcal{O}_7 &= \frac{e}{16\pi^2} \bar{m}_b (\bar{s} \sigma^{\mu\nu} P_R b) F_{\mu\nu}, & \mathcal{O}_8 &= \frac{g}{16\pi^2} \bar{m}_b (\bar{s}_{a_1} \sigma^{\mu\nu} P_R \mathbf{T}_{a_1 a_2} b_{a_2}) \mathbf{G}_{\mu\nu}, \\
\mathcal{O}_9 &= \frac{e^2}{16\pi^2} (\bar{s} \gamma^\mu P_L b) (\bar{\ell} \gamma_\mu \ell), & \mathcal{O}_{10} &= \frac{e^2}{16\pi^2} (\bar{s} \gamma^\mu P_L b) (\bar{\ell} \gamma_\mu \gamma_5 \ell),
\end{aligned} \tag{26}$$

where $\mathbf{G}_{\mu\nu}$ and $F_{\mu\nu}$ are the gluon and photon field strengths, respectively; $\mathbf{T}_{a_1 a_2}$ are the generators of the $SU(3)$ color group; a_1 and a_2 denote color indices (they are omitted in the color-singlet currents). The chirality projection operators are $P_{L,R} = (1 \mp \gamma_5)/2$ and μ is a renormalization scale. $\mathcal{O}_{1,2}$ are current-current operators, \mathcal{O}_{3-6} are QCD penguin operators, $\mathcal{O}_{7,8}$ are "magnetic penguin" operators, and $\mathcal{O}_{9,10}$ are semileptonic electroweak penguin operators. We denote the QCD quark masses by the bar symbol to distinguish them from the constituent quark masses used in the model.

By using the effective Hamiltonian defined by Eq. (25) one can write the matrix element of the exclusive transition $B_s \rightarrow \phi \ell^+ \ell^-$ as

$$\begin{aligned}
\mathcal{M} &= \frac{G_F}{\sqrt{2}} \cdot \frac{\alpha \lambda_t}{\pi} \cdot \left\{ C_9^{\text{eff}} \langle \phi | \bar{s} \gamma^\mu P_L b | B_s \rangle (\bar{\ell} \gamma_\mu \ell) \right. \\
&\quad - \frac{2\bar{m}_b}{q^2} C_7^{\text{eff}} \langle \phi | \bar{s} i \sigma^{\mu\nu} q_\nu P_R b | B_s \rangle (\bar{\ell} \gamma_\mu \ell) \\
&\quad \left. + C_{10} \langle \phi | \bar{s} \gamma^\mu P_L b | B_s \rangle (\bar{\ell} \gamma_\mu \gamma_5 \ell) \right\}, \tag{27}
\end{aligned}$$

where $C_7^{\text{eff}} = C_7 - C_5/3 - C_6$. One has to note that matrix element in Eq.(27) contains both a free quark decay amplitude coming from the operators \mathcal{O}_7 , \mathcal{O}_9 and \mathcal{O}_{10} (gluon magnetic penguin \mathcal{O}_8 does not contribute) and, in addition, certain long-distance effects from the matrix elements of four-quark operators \mathcal{O}_i ($i = 1, \dots, 6$) which usually are absorbed into a redefinition of the short-distance Wilson-coefficients. The Wilson coefficient C_9^{eff} effectively takes into account, first, the contributions from the four-quark operators \mathcal{O}_i ($i = 1, \dots, 6$) and, second, the nonperturbative effects coming from the $c\bar{c}$ -resonance contributions which

are as usual parametrized by the Breit-Wigner ansatz [40]:

$$\begin{aligned}
C_9^{\text{eff}} &= C_9 + C_0 \left\{ h(\hat{m}_c, s) + \frac{3\pi}{\alpha^2} \kappa \sum_{V_i=\psi(1s),\psi(2s)} \frac{\Gamma(V_i \rightarrow l^+l^-) m_{V_i}}{m_{V_i}^2 - q^2 - im_{V_i}\Gamma_{V_i}} \right\} \\
&- \frac{1}{2}h(1, s) (4C_3 + 4C_4 + 3C_5 + C_6) \\
&- \frac{1}{2}h(0, s) (C_3 + 3C_4) + \frac{2}{9} (3C_3 + C_4 + 3C_5 + C_6) ,
\end{aligned} \tag{28}$$

where $C_0 \equiv 3C_1 + C_2 + 3C_3 + C_4 + 3C_5 + C_6$. Here the charm-loop function is written as

$$\begin{aligned}
h(\hat{m}_c, s) &= -\frac{8}{9} \ln \frac{\bar{m}_b}{\mu} - \frac{8}{9} \ln \hat{m}_c + \frac{8}{27} + \frac{4}{9}x \\
&- \frac{2}{9}(2+x)|1-x|^{1/2} \left\{ \begin{array}{l} \left(\ln \left| \frac{\sqrt{1-x}+1}{\sqrt{1-x}-1} \right| - i\pi \right), \text{ for } x \equiv \frac{4\hat{m}_c^2}{s} < 1, \\ 2 \arctan \frac{1}{\sqrt{x-1}}, \text{ for } x \equiv \frac{4\hat{m}_c^2}{s} > 1, \end{array} \right. \\
h(0, s) &= \frac{8}{27} - \frac{8}{9} \ln \frac{\bar{m}_b}{\mu} - \frac{4}{9} \ln s + \frac{4}{9}i\pi,
\end{aligned}$$

where $\hat{m}_c = \bar{m}_c/m_1$, $s = q^2/m_1^2$ and $\kappa = 1/C_0$. In what follows we drop the charm resonance contributions by putting $\kappa = 0$. We will use the value of $\mu = \bar{m}_{b\text{pole}}$ for the renormalization scale. Besides the charm-loop perturbative contribution, two loop contributions have been calculated in [19, 20]. They effectively modify the Wilson coefficients as

$$\begin{aligned}
C_7^{\text{eff}} &\rightarrow C_7^{\text{eff}} - \frac{\alpha_S}{4\pi} \left(C_1 F_1^{(7)} + C_2 F_2^{(7)} \right), \\
C_9^{\text{eff}} &\rightarrow C_9^{\text{eff}} - \frac{\alpha_S}{4\pi} \left(C_1 F_1^{(9)} + C_2 F_2^{(9)} \right)
\end{aligned} \tag{29}$$

where the two-loop form factors $F_{1,2}^{(7,9)}$ are available in Ref. [20] as the Mathematica files.

The SM Wilson coefficients are taken from Ref. [6]. They were computed at the matching scale $\mu_0 = 2M_W$ and run down to the hadronic scale $\mu_b = 4.8$ GeV. The evolution of couplings and current quark masses proceeds analogously. The values of the model independent input parameters and the Wilson coefficients are listed in Table III.

A global analysis of $b \rightarrow sll$ anomalies has been performed in Ref. [4] with the Next-to-Next-to-Leading Logarithmic (NNLL) corrections included. It was shown that they amount up to 15%. The discussion of the non-local $c\bar{c}$ contributions maybe also found in Ref. [11].

TABLE III: Values of the input parameters.

m_W	$\sin^2 \theta_W$	$\alpha(M_Z)$	\bar{m}_c	\bar{m}_b	\bar{m}_t	λ_t			
80.41 GeV	0.2313	1/128.94	1.27 GeV	4.68 GeV	173.3 GeV	0.041			
C_1	C_2	C_3	C_4	C_5	C_6	C_7^{eff}	C_9	C_{10}	
-0.2632	1.0111	-0.0055	-0.0806	0.0004	0.0009	-0.2923	4.0749	-4.3085	

V. NUMERICAL RESULTS

We are aiming to compare our results for the branching fractions and angular observables with the experimental data recently reported by the LHCb Collaboration [3] and the results of global analyses performed in Ref. [4]. The four-fold distribution in the cascade decay $B \rightarrow \phi(\rightarrow K^+K^-)\bar{\ell}\ell$ allows one to define a number of physical observables which can be measured experimentally. The observables accessible in the decay $B_s \rightarrow \phi\mu^+\mu^-$ [3] are the CP averaged differential branching ratio $d\mathcal{B}/dq^2$, the CP-averaged ϕ longitudinal polarization fraction F_L , forward-backward asymmetry A_{FB} and the CP-averaged angular observables $S_{3,4,7}$ which may be related to the optimized observables P_i [4]. The CP asymmetries $A_{5,6,8,9}$ [41] in the SM are induced by the weak phase from the CKM matrix. For the $b \rightarrow s$ transitions the CP asymmetries are proportional to $\text{Im}(\hat{\lambda}_u) \equiv \text{Im}(V_{ub}V_{us}^*/V_{tb}V_{ts}^*)$ which is of order 10^{-2} [41]. The experimental data reported by [3] contain huge statistical uncertainties (see, Table 3 in [3]). For these reasons we restricted ourselves to the CP-averaged quantities.

We start with the branching fraction of the rare decay $B_s \rightarrow \phi\bar{\ell}\ell$. The width of this decay is computed by integration of the q^2 -differential distribution

$$\frac{d\Gamma(B \rightarrow \phi\bar{\ell}\ell)}{dq^2} = \frac{G_F^2}{(2\pi)^3} \left(\frac{\alpha\lambda_t}{2\pi}\right)^2 \frac{|\mathbf{p}_2| q^2 \beta_\ell}{12 m_1^2} \mathcal{H}_{\text{tot}},$$

$$\mathcal{H}_{\text{tot}} = \frac{1}{2} (\mathcal{H}_U^{11} + \mathcal{H}_U^{22} + \mathcal{H}_L^{11} + \mathcal{H}_L^{22}) + \delta_{\ell\ell} \left[\frac{1}{2} \mathcal{H}_U^{11} - \mathcal{H}_U^{22} + \frac{1}{2} \mathcal{H}_L^{11} - \mathcal{H}_L^{22} + \frac{3}{2} \mathcal{H}_S^{22} \right]. \quad (30)$$

In what follows we will use the short notation $m_1 = m_{B_s}$, $m_2 = m_\phi$, $\beta_\ell = \sqrt{1 - 4m_\ell^2/q^2}$, $\delta_{\ell\ell} = 2m_\ell^2/q^2$. Then $|\mathbf{p}_2| = \lambda^{1/2}(m_1^2, m_2^2, q^2)/(2m_1)$ is the momentum of the ϕ -meson given in the B_s -rest frame. The bilinear combinations of the helicity amplitudes \mathcal{H} are defined as

(see, Ref. [23] for details):

$$\mathcal{H}_U^i = |H_{+1+1}^i|^2 + |H_{-1-1}^i|^2, \quad \mathcal{H}_L^i = |H_{00}^i|^2, \quad \mathcal{H}_S^i = |H_{t0}^i|^2, \quad (31)$$

where the helicity amplitudes are expressed via the form factors appearing in the matrix element of the rare decay $B_s \rightarrow \phi \bar{\ell} \ell$ as

$$\begin{aligned} H_{t0}^i &= \frac{1}{m_1 + m_2} \frac{m_1 |\mathbf{p}_2|}{m_2 \sqrt{q^2}} (Pq (-A_0^i + A_+^i) + q^2 A_-^i), \\ H_{\pm 1 \pm 1}^i &= \frac{1}{m_1 + m_2} (-Pq A_0^i \pm 2 m_1 |\mathbf{p}_2| V^i), \\ H_{00}^i &= \frac{1}{m_1 + m_2} \frac{1}{2 m_2 \sqrt{q^2}} (-Pq (m_1^2 - m_2^2 - q^2) A_0^i + 4 m_1^2 |\mathbf{p}_2|^2 A_+^i). \end{aligned} \quad (32)$$

The form factors A^i and V^i ($i = 1, 2$) are related to the form factors in the $B_s - \phi$ transitions, see Eqs. (19) and (20), in the following manner

$$\begin{aligned} V^{(1)} &= C_9^{\text{eff}} V + C_7^{\text{eff}} g \frac{2\bar{m}_b(m_1 + m_2)}{q^2}, \\ A_0^{(1)} &= C_9^{\text{eff}} A_0 + C_7^{\text{eff}} a_0 \frac{2\bar{m}_b(m_1 + m_2)}{q^2}, \\ A_+^{(1)} &= C_9^{\text{eff}} A_+ + C_7^{\text{eff}} a_+ \frac{2\bar{m}_b(m_1 + m_2)}{q^2}, \\ A_-^{(1)} &= C_9^{\text{eff}} A_- + C_7^{\text{eff}} (a_0 - a_+) \frac{2\bar{m}_b(m_1 + m_2)}{q^2} \frac{Pq}{q^2}, \\ V^{(2)} &= C_{10} V, \quad A_0^{(2)} = C_{10} A_0, \quad A_{\pm}^{(2)} = C_{10} A_{\pm}. \end{aligned} \quad (33)$$

The differential rate of the decay $B_s \rightarrow \phi \nu \bar{\nu}$ is calculated according to

$$\frac{d\Gamma(B_s \rightarrow \phi \nu \bar{\nu})}{dq^2} = \frac{G_F^2}{(2\pi)^3} (\alpha \lambda_t)^2 \left[\frac{D_\nu(x_t)}{\sin^2 \theta_W} \right]^2 \frac{|\mathbf{p}_2| q^2}{4m_1^2} \cdot (H_U + H_L), \quad (34)$$

where $x_t = \bar{m}_t^2/m_W^2$ and the function D_ν is given by

$$D_\nu(x) = \frac{x}{8} \left(\frac{2+x}{x-1} + \frac{3x-6}{(x-1)^2} \ln x \right). \quad (35)$$

The relevant bilinear helicity combinations are defined as

$$\begin{aligned} \mathcal{H}_U &= |H_{+1+1}|^2 + |H_{-1-1}|^2, \quad \mathcal{H}_L = |H_{00}|^2, \\ H_{\pm 1 \pm 1} &= \frac{1}{m_1 + m_2} (-Pq A_0 \pm 2 m_1 |\mathbf{p}_2| V), \\ H_{00} &= \frac{1}{m_1 + m_2} \frac{1}{2 m_2 \sqrt{q^2}} (-Pq (m_1^2 - m_2^2 - q^2) A_0 + 4 m_1^2 |\mathbf{p}_2|^2 A_+). \end{aligned} \quad (36)$$

The width of the color-suppressed nonleptonic decay $B_s \rightarrow J/\psi \phi$ decay is given by [29]

$$\Gamma(B_s \rightarrow J/\psi \phi) = \frac{G_F^2 |\mathbf{P}_2|}{16\pi m_1^2} |V_{cb}V_{cs}|^2 (C_1^{\text{eff}} + C_5^{\text{eff}})^2 (m_{J/\psi} f_{J/\psi})^2 (H_U + H_L) \quad (37)$$

where the momentum transfer squared is taken on the mass of J/ψ , i.e. $q^2 = m_{J/\psi}^2$, $V_{cb} = 0.406$, $V_{cs} = 0.975$ and $f_{J/\psi} = 415$ MeV. The Wilson coefficients are combined as $C_1^{\text{eff}} = C_1 + \xi C_2 + C_3 + \xi C_4$ and $C_5^{\text{eff}} = C_5 + \xi C_6$ in accordance with the naive factorization. The terms multiplied by the color factor $\xi = 1/N_c$ will be dropped in the numerical calculations according to the $1/N_c$ -expansion.

Finally, we calculate the width of radiative decay $B_s \rightarrow \phi\gamma$ defined by

$$\Gamma(B_s \rightarrow \phi\gamma) = \frac{G_F^2 \alpha \lambda_t^2}{32\pi^4} \bar{m}_b^2 m_1^3 \left(1 - \frac{m_2^2}{m_1^2}\right)^3 |C_7^{\text{eff}}|^2 g^2(0). \quad (38)$$

One has to note that the experimental observables in the decays of neutral B_s -mesons are affected by $B_s - \bar{B}_s$ mixing. The theoretical framework for studying the time-dependent decays with taking into account such mixing has been recently developed in Ref. [42]. The mixing effects change the values of rates and CP averages within a few percents.

In Table IV the calculated values of branching fractions $B_s \rightarrow \phi\mu^+\mu^-$, $B_s \rightarrow \phi\tau^+\tau^-$, $B_s \rightarrow \phi\gamma$, $B_s \rightarrow \phi\nu\bar{\nu}$ and $B_s \rightarrow \phi J/\psi$ are given. The experimental errors shown in Table IV result from combining the partial uncertainties in quadrature. The model uncertainties are estimated to be within 10%. We compare our results with those obtained in other approaches.

TABLE IV: Total branching fractions.

	This work	Ref. [32]	Ref. [33]	Ref. [38]	Ref. [43]	Ref. [3, 44]
$10^7 \mathcal{B}(B_s \rightarrow \phi\mu^+\mu^-)$	9.11 ± 1.82	11.1 ± 1.1	19.2	11.8 ± 1.1	16.4	7.97 ± 0.77
$10^7 \mathcal{B}(B_s \rightarrow \phi\tau^+\tau^-)$	1.03 ± 0.20	1.5 ± 0.2	2.34	1.23 ± 0.11	1.51	
$10^5 \mathcal{B}(B_s \rightarrow \phi\gamma)$	2.39 ± 0.48	3.8 ± 0.4				3.52 ± 0.34
$10^5 \mathcal{B}(B_s \rightarrow \phi\nu\bar{\nu})$	0.84 ± 0.16	0.796 ± 0.080			1.165	< 540
$10^2 \mathcal{B}(B_s \rightarrow \phi J/\psi)$	0.16 ± 0.03	0.113 ± 0.016				0.108 ± 0.009

The full four-fold angular decay distribution for the rare B decay has been derived in Ref. [23] in terms of helicity amplitudes including lepton mass effects. It is described by the three angles and the squared momentum q^2 of the lepton pair. This distribution allows one to

define a number of physical observables which can be measured experimentally. Among them are three natural observables: the branching ratio, the longitudinal polarization fraction of the ϕ -meson and the forward-backward asymmetry. The differential branching fraction is obtained from the full four-fold angular decay distribution by integration over all three angles. The explicit expression is given by Eq. (30) in terms of helicity amplitudes. The relation of helicity amplitudes and the transversality amplitudes is obtained in Ref. [28].

The longitudinal polarization fraction and the forward-backward asymmetry are defined as

$$F_L = \frac{1}{2}\beta_\ell^2 \frac{\mathcal{H}_L^{11} + \mathcal{H}_L^{22}}{\mathcal{H}_{\text{tot}}}, \quad (39)$$

$$F_T = \frac{1}{2}\beta_\ell^2 \frac{\mathcal{H}_U^{11} + \mathcal{H}_U^{22}}{\mathcal{H}_{\text{tot}}}, \quad (40)$$

$$A_{\text{FB}} = \frac{1}{d\Gamma/dq^2} \left[\int_0^1 - \int_{-1}^0 \right] d\cos\theta \frac{d^2\Gamma}{dq^2 d\cos\theta} = -\frac{3}{4}\beta_\ell \frac{\mathcal{H}_P^{12}}{\mathcal{H}_{\text{tot}}}, \quad (41)$$

where θ is the polar angle between the $\ell^+\ell^-$ -plane and z-axis. As follows from the definition, the quantities A_{FB} and F_L are the ratios of the hadronic amplitudes which are supposed to be less dependent on the theoretical uncertainties.

The behavior of the differential branching fraction $d\mathcal{B}/dq^2$, forward-backward asymmetry A_{FB} and longitudinal polarization F_L is shown in Figs. 3, 4 and 5, respectively.

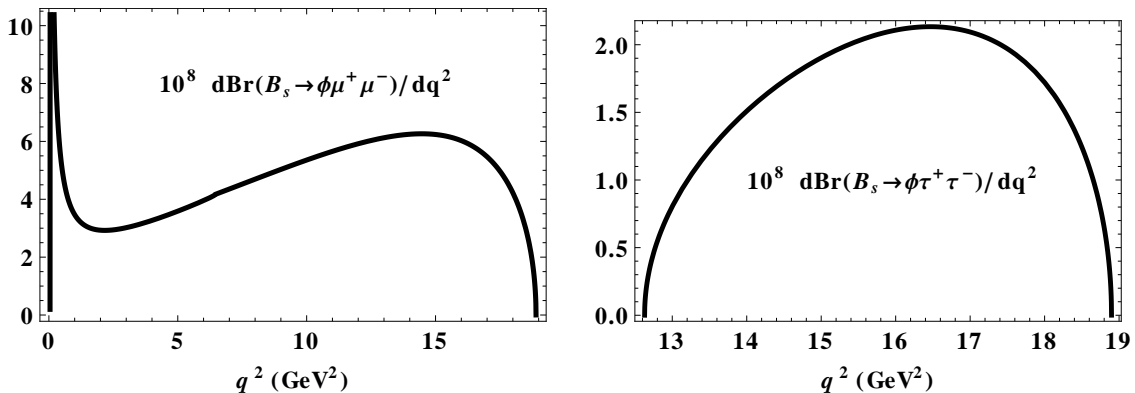


FIG. 3: Differential branching fraction in GeV^{-2} .

A set of so-called optimized observables P_i has been constructed (see [6] and references therein) by taking appropriate ratios of the form factors in such a way to minimize the hadronic uncertainties. These observables have been constructed with aim to reduce the

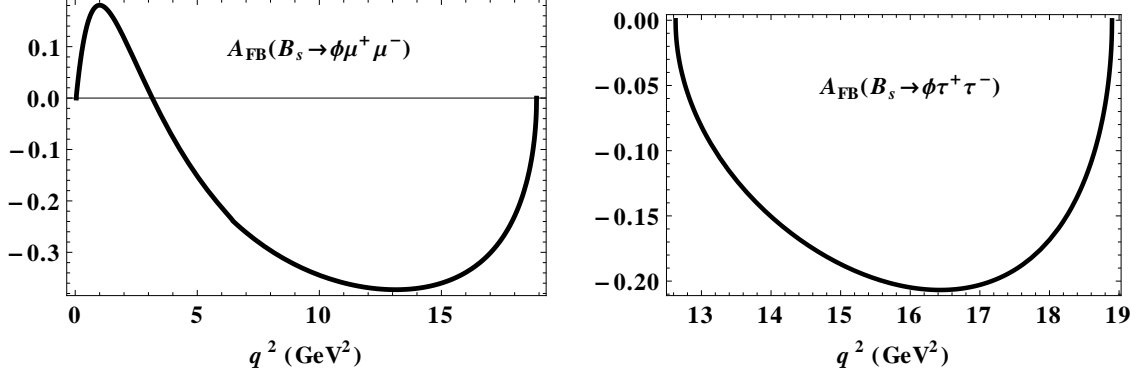


FIG. 4: Forward-backward asymmetry A_{FB} .

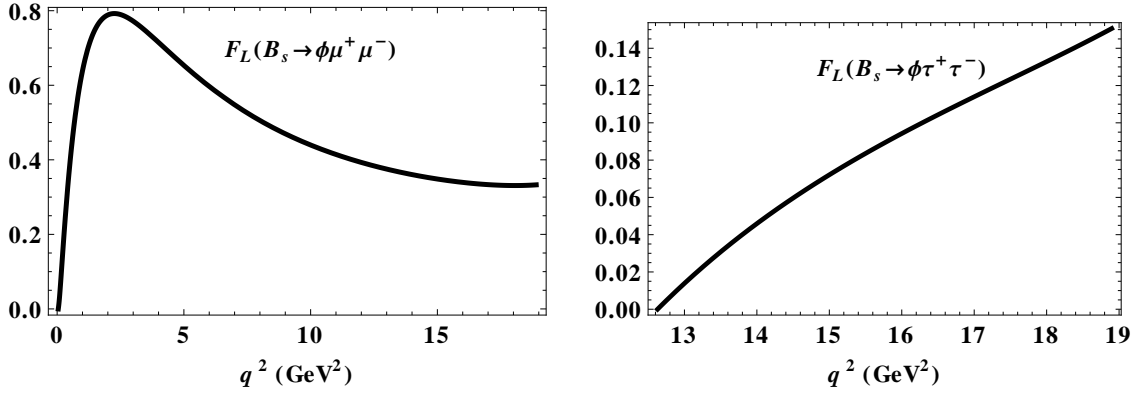


FIG. 5: Longitudinal polarization F_L .

form factor dependence and increase the discrimination power between the SM and NP, together with preserving a good experimental accessibility. It seems however more difficult to give them a clean physical interpretation, as it was the case for A_{FB} and F_L .

The optimized observables have not been given explicitly in [3]. Their numerical values were obtained in [4] by converting the results for the CP averages $S_{3,4,7}$ into the optimized observables.

We will calculate directly the optimized observables P_i expressed through the helicity amplitudes as was done in Ref. [28]. The q^2 -dependence of the optimized observables P_1 and P'_4 is displayed in Fig.6.

The q^2 -averages of polarization observables over the whole allowed kinematic region are given in Table V. For comparison reasons, we also give the values of the $S_{3,4,7}$ by using the relations [5]:

$$S_3 = \frac{1}{2}F_T P_1, \quad S_4 = \frac{1}{2}\sqrt{F_T F_L} P'_4, \quad S_7 = -\sqrt{F_T F_L} P'_6. \quad (42)$$

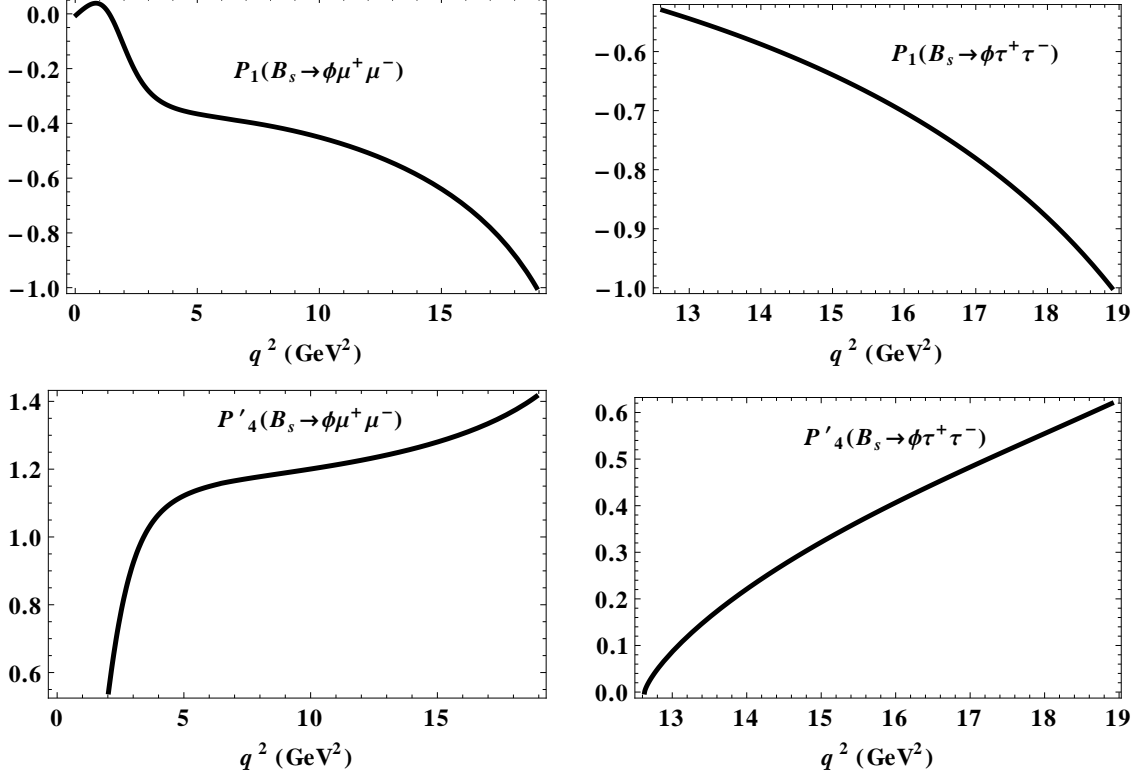


FIG. 6: Clean observables P_1 and P'_4 .

TABLE V: q^2 -averages of polarization observables over the whole allowed kinematic region.

$B_s \rightarrow \phi \ell^+ \ell^-$						
	$\langle A_{FB} \rangle$	$\langle F_L \rangle$	$\langle P_1 \rangle$	$\langle P'_4 \rangle$	$\langle S_3 \rangle$	$\langle S_4 \rangle$
μ	-0.24 ± 0.05	0.45 ± 0.09	-0.52 ± 0.1	1.05 ± 0.21	-0.14 ± 0.03	0.26 ± 0.05
τ	-0.18 ± 0.04	0.090 ± 0.02	-0.76 ± 0.15	1.33 ± 0.27	-0.067 ± 0.013	0.083 ± 0.017

We use the Wilson coefficients obtained at the next-to-leading logarithmic (NLL) order in our calculation of the observables in the full kinematical region of the momentum transfer squared. At this order only the coefficient C_9^{eff} has imaginary part. Since our form factors are real, the optimized observable P'_6 is identically zero at this order. The optimized observable P_1 is small for large recoil for any choice of the Wilson coefficients. It is easy to check that $P_1 \propto A_0(0) - V(0)$ at $q^2 = 0$. In our model $A_0(0) = 0.40$ and $V(0) = 0.31$ so it leads to the really small value of the P_1 . Note that $A_0(0) = V(0)$ in the heavy quark limit.

Finally, we present our results for the binned observables in Table VI. Here, we take

into account the NNLL corrections for the Wilson coefficients which have been calculated in [19, 20]. They effectively modify the Wilson coefficients C_7^{eff} and C_9^{eff} . The two-loop corrections to the decay $b \rightarrow s\ell^+\ell^-$ were given in [19] as expansions in the small parameters $\hat{s} = q^2/\bar{m}_b^2$ and $z = \bar{m}_c^2/\bar{m}_b^2$. The q^2 -region was restricted to the range $0.05 \leq \hat{s} \leq 0.25$. The NNLL corrections in the high q^2 region above the charm threshold $q^2 > 4\bar{m}_c^2$ were presented in [20]. The high q^2 -region was restricted to the range $0.4 \leq \hat{s} \leq 1.0$. By using the value of QCD bottom quark $\bar{m}_b = 4.68$ GeV from Table III one can obtain the q^2 regions where the two-loop corrections are valid:

$$1.1 \leq q^2 \leq 5.5 \text{ GeV}^2 \quad (\text{low region}) \quad \text{and} \quad 8.8 \leq q^2 \leq 22 \text{ GeV}^2 \quad (\text{high region}). \quad (43)$$

However, for the 2-loop calculation in the low q^2 region, it was important that q^2/\bar{m}_b^2 and $q^2/(4\bar{m}_c^2)$ are both much smaller than 1. So one can safely use the results of Ref. [19] for low q^2 in the region $0.1 \leq q^2 \leq 6 \text{ GeV}^2$. The two-loop expansion in the high q^2 region [20] can be justified only for $q^2/\bar{m}_b^2 > 0.4$. For this reason, we exclude the bin [5, 8] from the consideration of two-loop corrections [45].

Now the observable P'_6 and hence S_7 become different from zero. The NNLL corrections contribute up to 20% in the region of small transferred momentum squared $q^2 \leq 6 \text{ GeV}^2$ but their influence in the region of large q^2 is really negligible.

VI. DISCUSSION AND CONCLUSION

The level of agreement with experiment can be estimated by combining in quadrature the experimental errors with the theoretical ones: if the difference in observable values is smaller, then it can be seen as compatible with zero.

Using this optics one can address the 3.3σ deviation seen by [3] for branching fraction in the $1 - 6 \text{ GeV}^2$ range. In the covariant confined quark model this discrepancy is much reduced. The remaining deviation (0.9σ) shrinks even further if the two-loop corrections for the Wilson coefficients are taken into account, down to 0.7σ . With such error reduction one cannot claim a discrepancy with the SM any longer.

Overall one observes a good description of the data by the covariant quark model and the agreement becomes even better if the two-loop corrections are taken into account. The biggest discrepancy of 1.9σ observed for F_L in the lowest bin $0.1 \leq q^2 \leq 2 \text{ GeV}^2$ is reduced

to 1.4σ when these corrections are taken into account.

The remaining deviations do not exceed 1.7σ and only one of them is greater than 1.4σ if the two loops corrections are neglected (S_4 for $15 \leq q^2 \leq 17 \text{ GeV}^2$). When they are taken into account most measurements lie within one standard deviation, the only one exceeding 1.4σ is S_4 for $15 \leq q^2 \leq 17 \text{ GeV}^2$.

The largest deviation of the obtained results from the SM [4] predictions is found for the branching fraction at lower q^2 . One has to emphasize that the branching fraction is the most affected by the uncertainties related to the hadronic form factors. The global analysis performed in [4] has basically used a specific set of form factors determined from light-cone sum rules (LCSR) [13, 30, 31].

As discussed above, the value of P_1 at small q^2 is really small and lays within uncertainties given by both the experiment and global fit [4]. There is agreement between our approach and [4] for large q^2 . The values of P'_6 are identical zero at one-loop level. The results obtained by using two-loop expansion are in agreement with the experiment and with [4] within uncertainties.

One can conclude that the results provided by the covariant confined quark model do not allow to claim a significant deviation from the SM and they demonstrate the non-negligible effect of the two-loop corrections for the Wilson coefficients which bring the theoretical predictions closer to the data.

TABLE VI: Binned observables.

$10^7 \mathcal{B}(B_s \rightarrow \phi \mu^+ \mu^-)$	2 loop	1 loop	SM [4]	Expt. [3]
[0.1, 2]	0.99 ± 0.2	0.86 ± 0.17	1.81 ± 0.36	1.11 ± 0.16
[2, 5]	0.90 ± 0.18	0.95 ± 0.19	1.88 ± 0.31	0.77 ± 0.14
[5, 8]	--	1.25 ± 0.25	2.25 ± 0.41	0.96 ± 0.15
[11, 12.5]	0.84 ± 0.17	0.88 ± 0.18	--	0.71 ± 0.12
[15, 17]	1.15 ± 0.23	1.19 ± 0.24	--	0.90 ± 0.13
[17, 19]	0.75 ± 0.15	0.77 ± 0.15	--	0.75 ± 0.13
[1., 6.]	1.56 ± 0.31	1.64 ± 0.33	--	1.29 ± 0.19
[15, 19]	1.89 ± 0.28	1.95 ± 0.29	2.20 ± 0.16	1.62 ± 0.20
$F_L(B_s \rightarrow \phi \mu^+ \mu^-)$	2 loop	1 loop	SM [4]	Expt. [3]
[0.1, 2]	0.37 ± 0.07	0.46 ± 0.09	0.46 ± 0.09	0.20 ± 0.09
[2, 5]	0.72 ± 0.14	0.74 ± 0.15	0.79 ± 0.03	0.68 ± 0.15
[5, 8]	--	0.57 ± 0.11	0.65 ± 0.05	0.54 ± 0.10
[11, 12.5]	0.40 ± 0.08	0.40 ± 0.08	--	0.29 ± 0.11
[15, 17]	0.34 ± 0.07	0.34 ± 0.07	--	0.23 ± 0.09
[17, 19]	0.33 ± 0.06	0.33 ± 0.06	--	0.4 ± 0.14
[1, 6]	0.69 ± 0.14	0.71 ± 0.14	--	0.63 ± 0.09
[15, 19]	0.34 ± 0.07	0.34 ± 0.07	0.36 ± 0.02	0.29 ± 0.07
$P_1(B_s \rightarrow \phi \mu^+ \mu^-)$	2 loop	1 loop	SM [4]	Expt. [3]
[0.1, 2]	0.013 ± 0.003	0.012 ± 0.002	0.11 ± 0.08	-0.13 ± 0.33
[2, 5]	-0.26 ± 0.05	-0.31 ± 0.06	-0.10 ± 0.09	-0.38 ± 1.47
[5, 8]	--	-0.39 ± 0.08	-0.20 ± 0.10	-0.44 ± 1.27
[11, 12.5]	-0.50 ± 0.10	-0.50 ± 0.10	--	--
[15, 17]	-0.71 ± 0.14	-0.70 ± 0.14	--	--
[17, 19]	-0.86 ± 0.17	-0.86 ± 0.17	--	--
[1, 6]	-0.22 ± 0.04	-0.28 ± 0.06	--	--
[15, 19]	-0.77 ± 0.15	-0.77 ± 0.15	-0.69 ± 0.03	-0.25 ± 0.34

$P'_4(B_s \rightarrow \phi\mu^+\mu^-)$	2 loop	1 loop	SM [4]	Expt. [3]
[0.1, 2]	-0.18 ± 0.04	-0.15 ± 0.03	-0.28 ± 0.14	-1.35 ± 1.46
[2, 5]	0.86 ± 0.17	0.96 ± 0.19	0.80 ± 0.11	2.02 ± 1.84
[5, 8]	--	1.15 ± 0.23	1.06 ± 0.06	0.40 ± 0.72
[11, 12.5]	1.22 ± 0.24	1.22 ± 0.24	--	--
[15, 17]	1.31 ± 0.26	1.30 ± 0.26	--	--
[17, 19]	1.36 ± 0.27	1.36 ± 0.27	--	--
[1, 6]	0.75 ± 0.15	0.86 ± 0.17	--	--
[15, 19]	1.33 ± 0.26	1.33 ± 0.26	1.30 ± 0.01	0.62 ± 0.49
$P'_6(B_s \rightarrow \phi\mu^+\mu^-)$	2 loop	1 loop	SM [4]	Expt. [3]
[0.1, 2]	-0.016 ± 0.003	0	-0.06 ± 0.02	-0.10 ± 0.30
[2, 5]	-0.015 ± 0.003	0	-0.05 ± 0.02	0.06 ± 0.49
[5, 8]	--	0	-0.02 ± 0.01	-0.08 ± 0.40
[11, 12.5]	-0.0043 ± 0.0008	0	--	--
[15, 17]	-0.0018 ± 0.0004	0	--	--
[17, 19]	-0.00071 ± 0.00014	0	--	--
[1, 6]	-0.014 ± 0.003	0	--	--
[15, 19]	-0.0014 ± 0.0003	0	-0.00 ± 0.07	-0.29 ± 0.24
$S_3(B_s \rightarrow \phi\mu^+\mu^-)$	2 loop	1 loop	SM [4]	Expt. [3]
[0.1, 2]	0.0031 ± 0.0006	0.0023 ± 0.0005	0.02 ± 0.02	-0.05 ± 0.13
[2, 5]	-0.035 ± 0.007	-0.039 ± 0.008	-0.01 ± 0.01	-0.06 ± 0.21
[5, 8]	--	-0.082 ± 0.016	-0.03 ± 0.02	-0.10 ± 0.25
[11, 12.5]	-0.15 ± 0.03	-0.15 ± 0.03	--	-0.19 ± 0.21
[15, 17]	-0.23 ± 0.05	-0.23 ± 0.05	--	-0.06 ± 0.18
[17, 19]	-0.29 ± 0.06	-0.29 ± 0.06	--	-0.07 ± 0.25
[1, 6]	-0.034 ± 0.007	-0.039 ± 0.008	--	-0.02 ± 0.13
[15, 19]	-0.25 ± 0.05	-0.25 ± 0.05	-0.22 ± 0.01	-0.09 ± 0.12
$S_4(B_s \rightarrow \phi\mu^+\mu^-)$	2 loop	1 loop	SM [4]	Expt. [3]
[0.1, 2]	-0.038 ± 0.008	-0.031 ± 0.006	-0.06 ± 0.03	-0.27 ± 0.23
[2, 5]	0.19 ± 0.04	0.21 ± 0.04	0.16 ± 0.03	0.47 ± 0.37

[5, 8]	--	0.28 ± 0.06	0.25 ± 0.02	0.10 ± 0.17
[11, 12.5]	0.30 ± 0.06	0.30 ± 0.06	--	0.47 ± 0.25
[15, 17]	0.31 ± 0.06	0.31 ± 0.06	--	0.03 ± 0.15
[17, 19]	0.32 ± 0.06	0.32 ± 0.06	--	0.39 ± 0.3
[1, 6]	0.17 ± 0.03	0.19 ± 0.04	--	0.19 ± 0.14
[15, 19]	0.31 ± 0.06	0.31 ± 0.06	0.31 ± 0.00	0.14 ± 0.11
$S_7(B_s \rightarrow \phi\mu^+\mu^-)$	2 loop	1 loop	SM [4]	Expt. [3]
[0.1, 2]	0.0065 ± 0.0013	0	0.03 ± 0.01	0.04 ± 0.12
[2, 5]	0.0065 ± 0.0013	0	0.02 ± 0.01	-0.03 ± 0.21
[5, 8]	--	0	0.01 ± 0.00	0.04 ± 0.18
[11, 12.5]	0.0021 ± 0.0004	0	--	0.00 ± 0.16
[15, 17]	0.00087 ± 0.0002	0	--	0.12 ± 0.15
[17, 19]	0.00034 ± 0.00007	0	--	0.20 ± 0.26
[1, 6]	0.0065 ± 0.0013	0	--	-0.03 ± 0.14
[15, 19]	0.00066 ± 0.00013	0	0.00 ± 0.03	0.13 ± 0.11

Acknowledgments

We thank Christoph Greub and Javier Virto for useful discussions of some aspects of this work. This work was partly supported by the Slovak Grant Agency for Sciences VEGA, grant No. 1/0158/13 (S. Dubnička, A.Z. Dubničková, A. Liptaj), by the Slovak Research and Development Agency APVV, grant No. APVV-0463-12 (S. Dubnička, A.Z. Dubničková, A. Liptaj) and by Joint research project of Institute of Physics, SAS and Bogoliubov Laboratory of Theoretical Physics, JINR, No. 01-3-1114 (S. Dubnička, A.Z. Dubničková, M.A. Ivanov and A. Liptaj). A. Issadykov and M.A. Ivanov acknowledge the partial support by the Ministry of Education and Science of the Republic of Kazakhstan, grant 3092/GF4, state

- [1] R. Aaij *et al.* [LHCb Collaboration], Phys. Rev. Lett. **111**, 191801 (2013) [arXiv:1308.1707 [hep-ex]].
- [2] R. Aaij *et al.* [LHCb Collaboration], JHEP **1406**, 133 (2014) [arXiv:1403.8044 [hep-ex]].
- [3] R. Aaij *et al.* [LHCb Collaboration], JHEP **1509**, 179 (2015) [arXiv:1506.08777 [hep-ex]].
- [4] S. Descotes-Genon, L. Hofer, J. Matias and J. Virto, arXiv:1510.04239 [hep-ph].
- [5] S. Descotes-Genon, J. Matias, M. Ramon and J. Virto, JHEP **1301**, 048 (2013) [arXiv:1207.2753 [hep-ph]].
- [6] S. Descotes-Genon, T. Hurth, J. Matias and J. Virto, JHEP **1305**, 137 (2013) [arXiv:1303.5794 [hep-ph]].
- [7] S. Descotes-Genon, J. Matias and J. Virto, Phys. Rev. D **88**, 074002 (2013) [arXiv:1307.5683 [hep-ph]].
- [8] W. Altmannshofer and D. M. Straub, Eur. Phys. J. C **73**, 2646 (2013) [arXiv:1308.1501 [hep-ph]].
- [9] U. Egede, T. Hurth, J. Matias, M. Ramon and W. Reece, JHEP **1010**, 056 (2010) [arXiv:1005.0571 [hep-ph]].
- [10] M. Beneke, T. Feldmann and D. Seidel, Nucl. Phys. B **612**, 25 (2001) [hep-ph/0106067].
- [11] M. Beylich, G. Buchalla and T. Feldmann, Eur. Phys. J. C **71** (2011) 1635 [arXiv:1101.5118 [hep-ph]].
- [12] J. Lyon and R. Zwicky, arXiv:1406.0566 [hep-ph].
- [13] A. Bharucha, D. M. Straub and R. Zwicky, arXiv:1503.05534 [hep-ph].
- [14] A. Khodjamirian, T. Mannel, A. A. Pivovarov and Y.-M. Wang, JHEP **1009**, 089 (2010) [arXiv:1006.4945 [hep-ph]].
- [15] X. W. Kang, B. Kubis, C. Hanhart and U. G. Meiner, Phys. Rev. D **89**, 053015 (2014) [arXiv:1312.1193 [hep-ph]].
- [16] R. R. Horgan, Z. Liu, S. Meinel and M. Wingate, Phys. Rev. D **89**, no. 9, 094501 (2014) [arXiv:1310.3722 [hep-lat]].
- [17] R. R. Horgan, Z. Liu, S. Meinel and M. Wingate, Phys. Rev. Lett. **112**, 212003 (2014) [arXiv:1310.3887 [hep-ph]].

- [18] R. R. Horgan, Z. Liu, S. Meinel and M. Wingate, PoS LATTICE **2014**, 372 (2015) [arXiv:1501.00367 [hep-lat]].
- [19] H. H. Asatryan, H. M. Asatrian, C. Greub and M. Walker, Phys. Rev. D **65**, 074004 (2002) [hep-ph/0109140].
- [20] C. Greub, V. Pilipp and C. Schupbach, JHEP **0812**, 040 (2008) [arXiv:0810.4077 [hep-ph]].
- [21] G. V. Efimov and M. A. Ivanov, Int. J. Mod. Phys. A **4**, 2031 (1989).
- [22] G. V. Efimov and M. A. Ivanov, *The Quark Confinement Model of Hadrons*, (CRC Press, Boca Raton, 1993).
- [23] A. Faessler, T. Gutsche, M. A. Ivanov, J. G. Körner and V. E. Lyubovitskij, Eur. Phys. J. direct C **4**, 18 (2002) [hep-ph/0205287].
- [24] T. Branz, A. Faessler, T. Gutsche, M. A. Ivanov, J. G. Körner, V. E. Lyubovitskij, Phys. Rev. D **81**, 034010 (2010). [arXiv:0912.3710 [hep-ph]].
- [25] S. Weinberg, Phys. Rev. **130**, 776 (1963).
- [26] A. Salam, Nuovo Cimento **25**, 224 (1962).
- [27] K. Hayashi, M. Hirayama, T. Muta, N. Seto, and T. Shirafuji, Fortsch. Phys. **15**, 625 (1967).
- [28] S. Dubnička, A. Z. Dubničková, N. Habył, M. A. Ivanov, A. Liptaj and G. S. Nurbakova, Few Body Syst. **57**, no. 2, 121 (2016) [arXiv:1511.04887 [hep-ph]].
- [29] M. A. Ivanov, J. G. Körner, S. G. Kovalenko, P. Santorelli and G. G. Saidullaeva, Phys. Rev. D **85**, 034004 (2012) [arXiv:1112.3536 [hep-ph]].
- [30] A. Khodjamirian, T. Mannel and N. Offen, Phys. Rev. D **75**, 054013 (2007) [hep-ph/0611193].
- [31] P. Ball and R. Zwicky, Phys. Rev. D **71**, 014029 (2005) [hep-ph/0412079].
- [32] R. N. Faustov and V. O. Galkin, Eur. Phys. J. C **73**, no. 10, 2593 (2013) [arXiv:1309.2160 [hep-ph]].
- [33] U. O. Yilmaz, Eur. Phys. J. C **58** (2008) 555 [arXiv:0806.0269 [hep-ph]].
- [34] A. Ali, G. Kramer, Y. Li, C. D. Lu, Y. L. Shen, W. Wang and Y. M. Wang, Phys. Rev. D **76** (2007) 074018 [hep-ph/0703162 [HEP-PH]].
- [35] D. Melikhov and B. Stech, Phys. Rev. D **62** (2000) 014006 [hep-ph/0001113].
- [36] R. H. Li, C. D. Lu and W. Wang, Phys. Rev. D **79** (2009) 034014 [arXiv:0901.0307 [hep-ph]].
- [37] C. D. Lu, W. Wang and Z. T. Wei, Phys. Rev. D **76** (2007) 014013 [hep-ph/0701265 [HEP-PH]].
- [38] Y. L. Wu, M. Zhong and Y. B. Zuo, Int. J. Mod. Phys. A **21** (2006) 6125 [hep-ph/0604007].

- [39] G. Buchalla, A. J. Buras and M. E. Lautenbacher, Rev. Mod. Phys. **68**, 1125 (1996) [hep-ph/9512380].
- [40] A. Ali, T. Mannel, T. Morozumi: Phys. Lett. B **273** 505 (1991).
- [41] C. Bobeth, G. Hiller and G. Piranishvili, JHEP **0807**, 106 (2008) [arXiv:0805.2525 [hep-ph]].
- [42] S. Descotes-Genon and J. Virto, JHEP **1504**, 045 (2015) [JHEP **1507**, 049 (2015)] [arXiv:1502.05509 [hep-ph]].
- [43] C. Q. Geng and C. C. Liu, J. Phys. G **29** (2003) 1103 [hep-ph/0303246].
- [44] K. A. Olive *et al.* [Particle Data Group Collaboration], Chin. Phys. C **38**, 090001 (2014).
- [45] We appreciate Christoph Greub for discussion of these points.